JOURNAL OF MATERIALS SCIENCE **38** (2003) 3223–3231

Short-term flexural creep deformation in synroc-C

B. A. LATELLA, T. LIU, K. U. SNOWDEN, E. G. MEHRTENS, G. R. LUMPKIN
Materials and Engineering Science, Australian Nuclear Science and Technology Organisation, Private Mail Bag 1, Menai, NSW 2234, Australia
E-mail: bal@ansto.gov.au

B. K. GAN
Department of Applied and Plasma Physics, School of Physics, The University of Sydney, Sydney, NSW 2006, Australia

The flexural creep behaviour of synroc-C in an inert atmosphere was studied at temperatures of 860°C, 900°C and 940°C under constant-load conditions in four-point bending. Applied stresses ranged from 100 to 160 MPa. Individual creep curves show primary and secondary creep but little or no tertiary creep stage. The log of the creep rate was found to increase linearly with log of the applied stress at each temperature over the entire stress range. Analysis of the creep data using the Norton power-law function revealed that the stress exponent decreased from 3.3 ± 0.6 for the 860°C and 900°C data to 2.0 ± 0.2 for the 940°C data, and an activation energy of 440 ± 40 kJ/mol was obtained over the entire temperature and stress range. Comparative analysis with the theta-projection equation was found to adequately represent the data yielding an activation energy of 464 kJ/mol while also showing a trend for the stress exponent to decrease with increasing temperature. Microstructural examination revealed extensive cavitation on the tensile surface of the creep specimens subjected to higher stresses at 900°C and 940°C. Dynamic high temperature X-ray diffraction analysis indicated little change in the phase assemblage apart from a slight reduction in the amount of the hollandite phase at higher temperatures which was attributed to a minor amount of oxidation. The possible creep damage mechanism was explored with reference to creep test results and microstructural modifications and the implications of the observations are discussed.

1. Introduction

The reprocessing of spent fuel from nuclear power reactors produces high-level waste (HLW), which takes the form of highly-radioactive and acidic liquid-waste streams. A dense, fine-grained polyphase titanate ceramic commonly referred to as synroc [1, 2] has been developed to immobilise a range of HLW elements (for example, commercial or defense waste) to reduce the risk of radioactive leakage in long term storage.

For underground storage of HLW, the stability and durability of synroc to withstand severe chemical and thermal conditions, particularly in the context of radiation damage and leaching, is paramount. The high temperature mechanical response and creep behaviour are significant factors in the durability of synroc, and are of interest in regard to damage susceptibility if subjected to the higher reaches of planned repository design temperatures. Cracking and void formation could dramatically influence leach rates via geometrical effects. Consequently, obtaining basic creep information is important in assessing the long-term load-bearing capacity of the material and in the design for hot-pressing containers.

An earlier creep study in our laboratory was carried out on a similar synroc material [3] and performed under flowing (dynamic) argon atmosphere conditions although oxidation of the material occurred. Microstructural analysis was limited to oxidation effects and creep mechanism(s) were not identified. Accordingly, in this study creep tests were performed in a static argon environment where oxidation effects have been minimised and an analysis of the microstructural creep damage behaviour was carried out using scanning electron microscopy. It is important to note that apart from the work conducted in our laboratory there have been no other reported creep measurements on such a material in the literature.

The specific objectives of this investigation were: (i) to examine the flexural creep behaviour of the simulated (non-radioactive) form synroc-C, designed for HLW from PUREX-type reprocessing (Pu-U Recovery EXtraction), (ii) to provide essential data for hot

pressing container design/analysis and (iii) to examine possible creep damage mechanism(s).

2. Experimental procedure

2.1. Materials and preparation

The synroc-C formulation was processed using the alkoxide/nitrate route [2] and contained 18% PW-4b-C simulated waste. Processing and fabrication information are detailed elsewhere [4]. Specimens were prepared in the form of bend bars of dimensions 3.5 × 4.5 × 50 mm with the surfaces machined to a 10 μm finish and chamfered edges along one face to avoid edge failures. The material is the same as that used in an earlier study of the high temperature strength properties [4].

2.2. Flexural creep testing

Creep tests on the synroc bars were conducted using a fully articulated Si_3N_4 four-point bend fixture with free-rolling pins, inner span 20 mm and outer span 40 mm. Specimens were placed in position on the test jig with the chamfered edges forming the tension surface of the test specimen. The fixture was centrally located in a furnace cavity attached to the loading frame, via a moveable high-purity alumina rod, of a servo-electrically driven universal testing machine (Instron, 8561).

The chamber was evacuated to a pressure of 0.005 Torr (0.665 Pa) and flushed with commercial grade high purity argon (>99.995% purity, BOC Gases). The specimens were then heated using a single zone Kanthal A1 furnace at 5°C/min to the desired test temperature with a dwell time of 30 min to assure uniformity of sample temperature. The specimen was then loaded to the required stress level.

It was established that synroc displays considerable plastic deformation above 900°C with a strength peak around 940°C. Significant creep activity for the material starts at approximately 900°C; at 1000°C the creep of the material is relatively rapid, with failure occurring within a few hours. Based on these observations, creep experiments were conducted at 860°C, 900°C and 940°C. At each of these temperatures four applied stress levels (σ_{el} = 100, 120, 140, 160 MPa) were used, the magnitudes corresponding to about 1/3–1/2 of the breaking stress at 940°C [4]. A nominal maximum creep test time of ≈168 h or 7 days was used to provide an adequate representation of the creep behaviour. The loading point displacement during creep was monitored with a spring-loaded linear voltage displacement transducer (LVDT) attached to an alumina extension rod directly in contact with the centre of the tension face of the bend bar. The loading point displacement of specimens was measured to within ±2.5 μm. Temperature, load and displacement parameters were logged automatically using a computerised data acquisition system.

In addition to the creep tests, *in situ* high temperature X-ray diffraction (XRD) experiments in vacuum were performed to gauge changes in the phase assemblage of the material between 20°C and 1100°C. A small amount of the as-hot pressed material was crushed to a fine powder and then dispersed as a very thin layer on a sheet of platinum foil. The foil was placed in a dedicated high temperature XRD attachment, which was then evacuated to a pressure (<0.005 torr). An R-type thermocouple was placed close to the foil for temperature measurements. Diffraction patterns were acquired with a Siemens D5000 instrument using the following operating conditions: Cu K_α radiation (λ = 1.5418 Å) produced at 40 kV and 30 mA, 1° divergence for the incident beam and 0.15° receiving slit, goniometer range 5°–100°, step size = 0.02°, counting time = 3 s/step and postdiffraction graphite monochromator with NaI detector and pulse discrimination. A room temperature pattern was acquired and then the sample was heated in steps to selected temperatures and patterns collected. Crystalline phases in the specimen were identified by search-match analysis using the International Centre for Diffraction Data (ICDD) database. XRD analysis was also conducted for several specimens, before and after creep testing, to ascertain whether any oxidation had occurred.

2.3. Analysis

The creep test specimens in four-point bending were maintained at a constant load (P) in order to give a symmetric maximum elastic fibre stress of:

$$\sigma_{el} = 1.5P(L_o - L_i)/wh^2 \quad (1)$$

where L_i is the inner span width (mm), L_o is the outer span width (mm), w is the specimen width (mm) and h is the specimen thickness (mm). Creep data are generally plotted in terms of a relaxed symmetric stress, σ_{sym}, for four-point bending [5]:

$$\sigma_{sym} = \sigma_{el}[(2n + 1)/3n] \quad (2)$$

where n is the stress exponent in a Norton–Arrhenius type power law creep rate equation of the form:

$$\varepsilon' = A\sigma^n \exp(-Q/RT) \quad (3)$$

where ε' is the minimum strain rate or secondary creep rate in s^{-1}, σ is the stress in MPa, T is the absolute temperature in K, R is the universal gas constant, Q is the apparent creep activation energy in kJ/mol and A is a material constant. A problem with the bending creep of ceramics is that the neutral axis may deviate towards the compression surface of the beam resulting in a stress redistribution [3]. Therefore, a geometry-dependent "reference stress" [6] is used:

$$\sigma_{ref} = 1/6\sigma_{el}[(2n + 1)/n]^{n/(n+1)} \quad (4)$$

Strain (ε) was determined from the centre point deflection (δ) of the sample under load as measured by the LVDT:

$$\varepsilon = 12h\delta/\left[2L_o^2 + 2L_oL_i - L_i^2\right] \quad (5)$$

The creep rate or strain rate (ε') was determined by conducting a moving derivative calculation at a fixed step in deflection from the strain-time data. The minimum creep rate could then be obtained from the strain rate-time data.

2.4. Creep damage observations

Deformed test bars were cut parallel and perpendicular to the stress axis so that the surfaces exposed to tensile and compressive stresses were examined for creep damage by scanning electron microscopy (SEM). The samples were mounted in epoxy resin and then polished to a 0.25 μm finish using diamond paste. Subsequently the samples were coated with a thin layer of carbon and then viewed in a JEOL JSM-6400 scanning electron microscope equipped with energy dispersive spectroscopy (EDS) using a microanalysis system (NORAN Voyager).

3. Results

3.1. Microstructure of the material

The microstructure of the material used in the present study is similar to other synroc grades examined previously in our laboratory [2, 3], and a typical example of a polished section of synroc-C is shown in Fig. 1. It consists of a fine-grained ($\approx$1 μm) multiphase crystalline matrix along with a small concentration of dark grey TiO_{2-x} agglomerates about 30–40 μm in size derived from a 2 wt% Ti metal addition to the calcined powder before hot pressing. There is some porosity within these TiO_{2-x} relics. Room temperature XRD and EDS analysis identified hollandite ($BaAl_2Ti_6O_{16}$; 30 vol%), perovskite ($CaTiO_3$; 20 vol%), zirconolite ($CaZrTi_2O_7$; 30 vol%), rutile (TiO_2; 15 vol%) and metallic alloys ($\approx$5 vol%) and a minor amount of hibonite ($CaAl_{12}O_{19}$). A transmission electron microscopy (TEM) study on an equivalent synroc to that used in the present work indicated no amorphous phases at interstices between grains or at triple point junctions [7].

3.2. High temperature X-ray diffraction

The sequence of XRD patterns collected on heating the synroc material to 1100°C is shown in Fig. 2. The patterns are offset for clarity. The platinum (Pt) peaks are from the foil holder used in the experiment. There are subtle changes in the crystalline phase assemblage with increasing temperature. A distinguishing feature of the sequence of patterns in Fig. 2 is the slight peak shift towards lower angles with increasing temperature due to thermal expansion. Likewise the only perceptible change in the spectra is a reduction and broadening in the hollandite peaks with increasing temperature most likely due to a small amount of oxidation a symptom of which leads to an enhancement of the rutile peaks, although this is not entirely conclusive. The attenuation and broadening of the hollandite peaks at 1100°C is most obvious for the reflections at $2\theta = 25^\circ$ and 58°. Overall, the effect of the hollandite oxidation on the creep behaviour at the temperatures of interest in this study appears to be minimal.

3.3. Stress and temperature dependence of creep

Typical creep curves of the synroc material obtained at 860°C, 900°C and 940°C at an applied stress of 100 MPa are shown in Fig. 3. The 860°C and 900°C curves exhibit a continuously decreasing creep strain

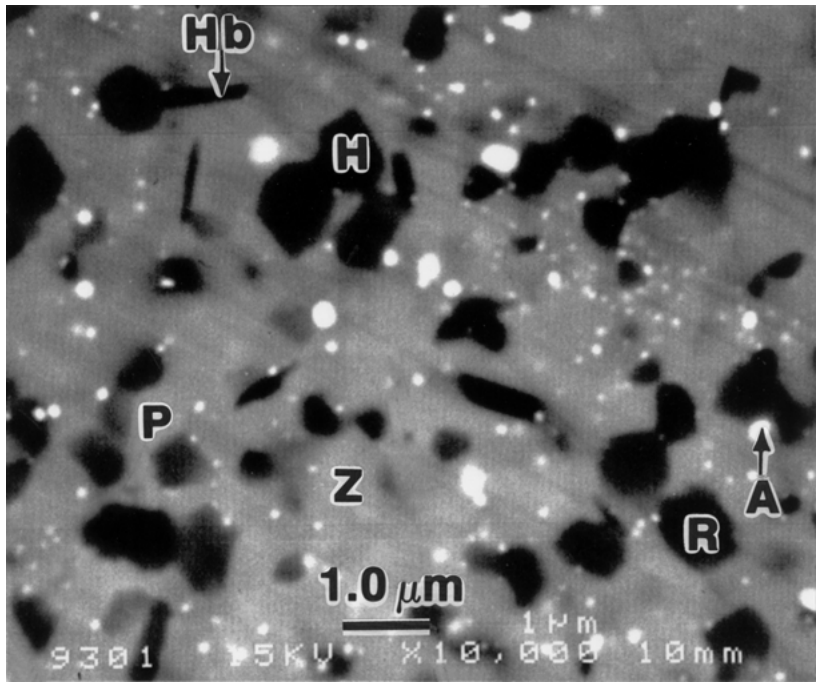

Figure 1 SEM (backscattered) microstructure of a polished section of synroc-C. The phases are labelled: H = Hollandite, Hb = Hibonite, R = Rutile, P = Perovskite, Z = Zirconolite and A = Alloys.

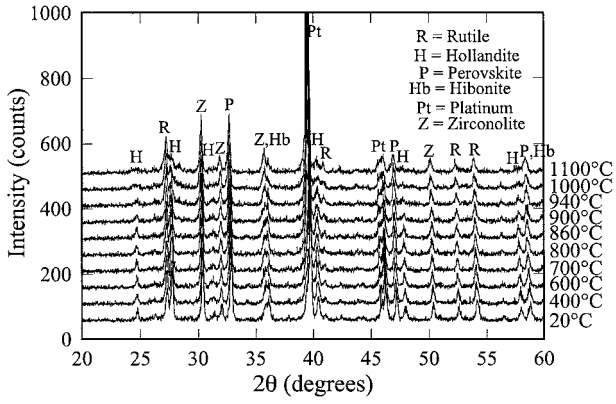

Figure 2 *In situ* XRD spectra of synroc-C heated in vacuum showing the complete sequence of patterns from room temperature to 1100°C. Patterns offset for clarity. The platinum (Pt) peaks are due to the sample holder.

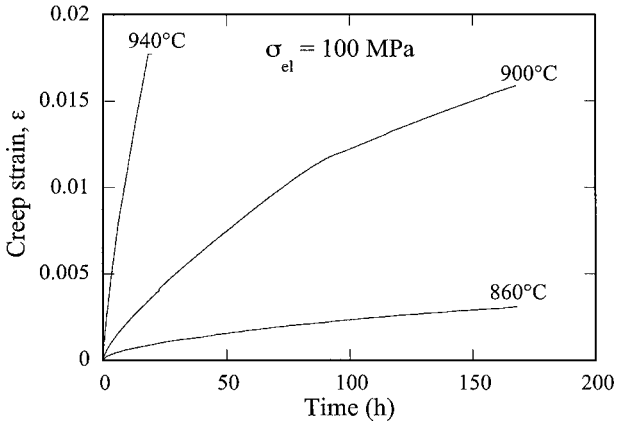

Figure 3 Typical creep curves for synroc-C at temperatures of 860°C, 900°C and 940°C at 100 MPa.

with time whereas the 940°C data exhibits a sharp rise in creep strain. The creep resistance decreases with increasing temperature and applied stress. Although the material exhibits significant creep activity (primary and secondary creep) no failures were observed for the temperatures and stress levels investigated, i.e., there was little if any sign of a tertiary stage detectable in any test. Repeat creep tests gave similar results indicating good reproducibility in the measured data.

In order to emphasise the initial creep behaviour, selected data (at $\sigma_{el} = 120$ MPa) for each temperature are presented in Fig. 4a in terms of creep strain rate as a function of creep strain on a log-log plot. For the 860°C data the creep rate shows a discernible linear decrease at all applied stresses. By contrast, at 900°C and 940°C the creep rates show a relatively minor but gradual linear decrease (for less than 0.7% creep strain) with a sharp drop evident for the 940°C data at higher strain. In Fig. 4b the strain rate data for each of these temperatures are replotted as a function of time. This shows the secondary stage of creep with a plateau in the data for 860°C and 900°C signifying a definite minimum creep rate.

Fig. 5 shows the stress dependency of the minimum creep rate for synroc as function of the relaxed and reference stresses. The solid lines through the data points are the best force fits to the Norton equation

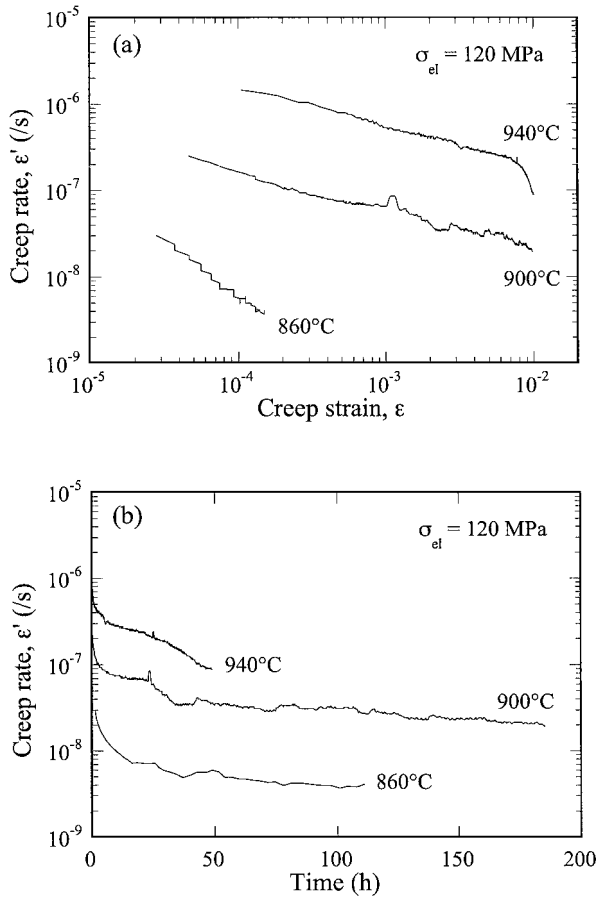

Figure 4 (a) Creep rate as a function of creep strain data for applied stress of 120 MPa at 860°C, 900°C and 940°C and (b) the corresponding creep rate versus time data.

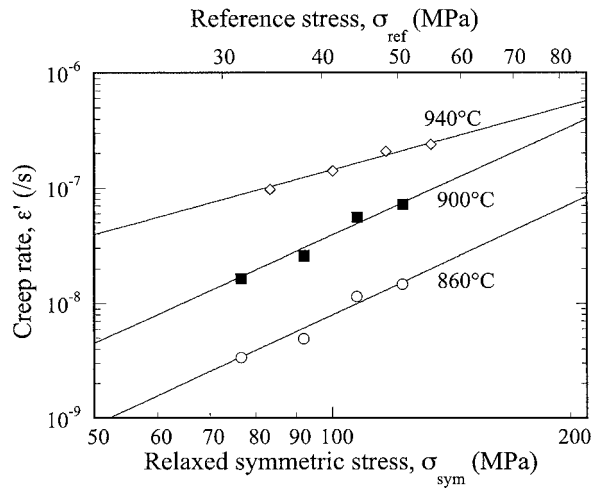

Figure 5 Creep rate versus the relaxed and the reference stresses for synroc-C at the designated testing temperatures. The solid lines represent the fit of Equation 3 to the experimental data.

(Equation 3) from which the constants A, n and Q may be obtained (refer to Section 3.4). The creep behaviour can be described well by the Norton power-law representation with creep rate increasing dramatically with increasing stress and temperature. Table I summarises all of the experimental creep data obtained in the tests. Data for the 940°C experiments were not collected for the full 7 days to avoid damage to the LVDT because of restricted movement.

TABLE I Summary of creep test data

Temperature T (°C)	Applied stress, σ_{el} (MPa)	Relaxed symmetric stress, σ_{sym} (MPa)	Reference stress, σ_{ref} (MPa)	Final creep strain, ε_f	Minimum creep rate, ε' 10^{-9} (s^{-1})	Total creep time (h)
860	100	76.6	31.6	0.0031	3.38	167.7
860	120	91.9	37.9	0.0015	4.95	139.1
860	140	107.3	44.3	0.0081	11.5	167.9
860	160	122.6	50.6	0.0133	14.7	167.8
900	100	76.7	31.6	0.0159	16.5	167.4
900	120	92.0	37.9	0.0242	25.9	186.3
900	140	107.4	44.3	0.0242	55.8	168.0
900	160	122.7	50.6	0.0299	71.9	167.7
940	100	83.4	30.7	0.0178	96.7	19.6
940	120	100.1	36.8	0.0390	141	49.2
940	140	116.7	42.9	0.0342	208	26.4
940	160	133.5	49.1	0.0386	238	26.0

3.4. Analysis of creep data

In the present experiment the constants A, n and Q were determined by a least-squares fit to the logarithmic representation of Equation 3:

$$\ln \varepsilon'_{min} = \ln A + n \ln \sigma - Q/RT \quad (6)$$

The linear regressions performed yielded values for n, Q and A which are given in Table II. An average activation energy $Q = (442 \pm 40)$ kJ/mol for all temperatures was obtained. Note that there is a large difference in the stress exponents for the 860°C/900°C and 940°C creep tests. This difference in the stress exponent at 940°C compared with 860°C and 900°C tends to suggest a different creep mechanism becomes dominant at the higher temperature. Therefore, two Norton creep equations are given below to describe the creep behaviour based on the fitted data; for 860°C and 900°C (assigned LT, low temperature) and for 940°C (assigned HT, high temperature):

$$\varepsilon'_{LT} = (1.73 \pm 0.27) \times 10^5 \sigma^{3.33 \pm 0.63} \times \exp(-(442 \pm 40)/RT) \quad (7)$$

$$\varepsilon'_{HT} = (1.17 \pm 0.06) \times 10^8 \sigma^{1.99 \pm 0.19} \times \exp(-(442 \pm 40)/RT) \quad (8)$$

The creep data were also analysed and fitted with a truncated form of the θ-projection equation of Evans and Wilshire [8, 9] given that there was no discernible tertiary creep:

$$\varepsilon = \theta_1(1 - \exp(-\theta_2 t)) + \theta_3\theta_4 t \quad (9)$$

TABLE II Norton power-law creep results from linear regression analysis

Temperature, T (°C)	n	A
860	3.35 ± 0.49	1.728×10^5
900	3.32 ± 0.39	1.724×10^5
940	1.99 ± 0.19	1.171×10^8
Applied stress, σ_{el} (MPa)	**Q (kJ/mol)**	
100	478 ± 25	
120	478 ± 13	
140	414 ± 14	
160	399 ± 25	

where θ_i are the theta parameters i = 1 to 4 and t is the time. The θ_1 parameter scales the primary strain, the θ_2 parameter is the rate parameter governing the curvature of the primary stage and $\theta_3\theta_4$ is the steady-state or long-term creep rate and can be treated as a single parameter. The quality of the fits to Equation 9 to the creep data were good and gave correlation coefficients better than $R^2 > 0.99$, the results of which are summarised in Table III.

It follows that the instantaneous creep rate is given by:

$$\varepsilon' = \theta_1\theta_2 \exp(-\theta_2 t) + \theta_3\theta_4 \quad (10)$$

The influence of stress and temperature on the θ_i terms can be described using:

$$\ln \theta_i = a_i + b_i\sigma + c_i T + d_i\sigma T \quad (11)$$

where σ is the stress in MPa and T is the temperature in K. Fitting Equation 11 to the data for $\ln \theta_i$ as shown in Table III gives:

$$\ln \theta_1 = -28.143 + 0.0361\sigma + 0.0179T - 4.2718 \times 10^{-6}\sigma T \quad (12a)$$

$$\ln \theta_2 = -14.306 - 0.00897\sigma + 0.0112T - 3.7789 \times 10^{-7}\sigma T \quad (12b)$$

$$\ln \theta_3\theta_4 = -100.94 + 0.3717\sigma + 0.0771T - 3.0558 \times 10^{-4}\sigma T \quad (12c)$$

Equations 12a, 12b and 12c can be used to calculate the values of θ_i at any stress and temperature. Similarly, these calculated θ_i can be used to estimate the creep strain and creep rate at time t. The validity of Equations 9 to 12 was checked by calculating the creep strains and the creep rates at the end of each test and compared to the actual values taken from each fitted creep curve. It was found that there was excellent agreement between the calculated and actual values, which lends confidence in the use of the theta equations.

The creep rates calculated from the theta coefficients obtained using Equation 10 were used to determine stress exponents at constant temperature, allowing for an expanded range of stresses (80 MPa to 180 MPa)

TABLE III Summary of calculated theta projection coefficients for creep test data

Temperature, T (°C)	Applied stress, σ_{el} (MPa)	θ_1	θ_2	$\theta_3\theta_4$	R^2
860	100	0.0010106	0.058746	1.28×10^{-5}	0.9975
860	120	0.00072534	0.10223	1.56×10^{-5}	0.9977
860	140	0.0013171	0.087643	4.06×10^{-5}	0.9996
860	160	0.0049601	0.028929	5.08×10^{-5}	0.9989
900	100	0.0018507	0.091863	0.00011231	0.9993
900	120	0.00092318	0.59905	0.00025635	0.9997
900	140	0.007502	0.052501	2.41×10^{-5}	0.9997
900	160	0.0055836	0.084444	0.00026523	0.9938
940	100	0.0034331	0.35621	0.00078751	0.9995
940	120	0.016384	0.077286	0.00049391	0.9982
940	140	0.015717	0.18874	0.00074865	0.9987
940	160	0.020561	0.12431	0.00074696	0.9989

outside the range of the experimental data for calculations to be performed adequately, using the following relation [8]:

$$n = \partial \ln \varepsilon' / \partial \ln \sigma \tag{13}$$

The n values were determined from the slope of $\ln \varepsilon'$ versus $\ln \sigma$ curves for each pair of points at each temperature. Fig. 6 shows n as a function of the midpoint stress at each temperature indicating stress exponent dependencies in accord with that obtained from the Norton equation, i.e., a change in slope between 900°C and 940°C. Similarly, the variation of $\theta_3\theta_4$ with stress and temperature can be described using [8]:

$$\theta_3\theta_4 = G_{3,4} \exp -((Q_{3,4} - H_{3,4}\sigma)/RT) \tag{14}$$

where $G_{3,4}$ and $H_{3,4}$ are constants, $Q_{3,4}$ are the activation energies associated with $\theta_3\theta_4$. The superimposition of the $\sigma - \ln \theta_3\theta_4$ data was obtained with $Q = (Q_{3,4} - H_{3,4}\sigma) = (464499 + 57.273\sigma)$ which indicates that the stress dependence of the activation energy is small and the deformation mechanisms are most likely the same over the range of stresses investigated. Consequently an activation energy of 464 ± 48 kJ/mol is obtained from the θ-projection analysis which is in agreement with that determined using the Norton power law equation (Equation 3, $Q = 442 \pm 40$ kJ/mol) and an estimate of 460 kJ/mol based on a correlation between lattice diffusion and the elastic modulus [3].

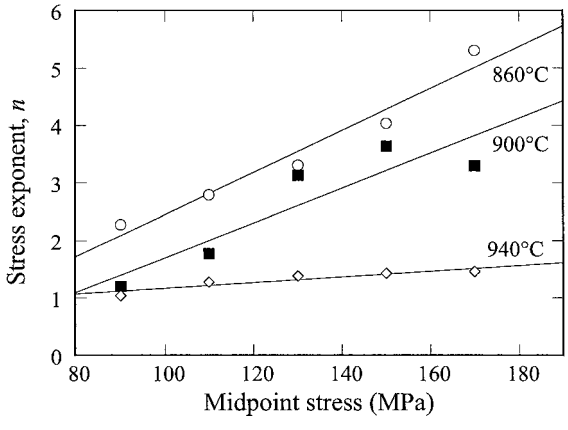

Figure 6 Variation of stress exponent, n, as a function of midpoint stress at each designated temperature. The solid lines are linear least squares fits to the data.

It is important to note that the creep mechanisms cannot always be reliably deduced from creep data alone because of complex interactions between microstructural constituents [10]. For this reason, creep mechanisms in the materials were examined by comparing the measured creep response with observations of the creep-damaged microstructures using SEM as will be shown in the next section.

3.5. Creep damage

SEM was performed on one sample from each of the test temperatures (860°C, 900°C and 940°C) subjected to an applied stress of 140 MPa. For each sample, sections from compressive, tensile and normal (outside the stressed area) regions were examined. EDS analysis indicated that the spectra (and hence phases) of the materials tested at each temperature were typical of synroc-C with no evidence of oxidation products (as is expected in the static Ar environment [4] and confirmed by XRD observations of tested samples.

Fig. 7 shows selected areas from the tensile areas of the samples tested at 860°C, 900°C and 940°C at σ_{el} = 140 MPa.

(i) At 860°C (Fig. 7a): there is no obvious evidence of creep deformation, shape change of individual grains (grains remain equiaxed) or cavitation in the tensile region compared to the normal area.

(ii) At 900°C (Fig. 7b): some small isolated cavities (<1 μm in size) are now evident on the tensile side. There is no associated cracking but the cavities appear to form along phase grain-boundary junctions. Moreover, it appears that cavity nucleation begins at about 900°C.

(iii) At 940°C (Fig. 7c): as with the 860°C and 900°C materials the micrographs of the normal and compressive regions do not show any irregularities. However, the tensile surface clearly shows a large amount of cavities scattered throughout the microstructure. As with the 900°C sample there are some small isolated cavities (<1 μm in size) but also larger cavities forming at grain-boundary junctions and growing from these

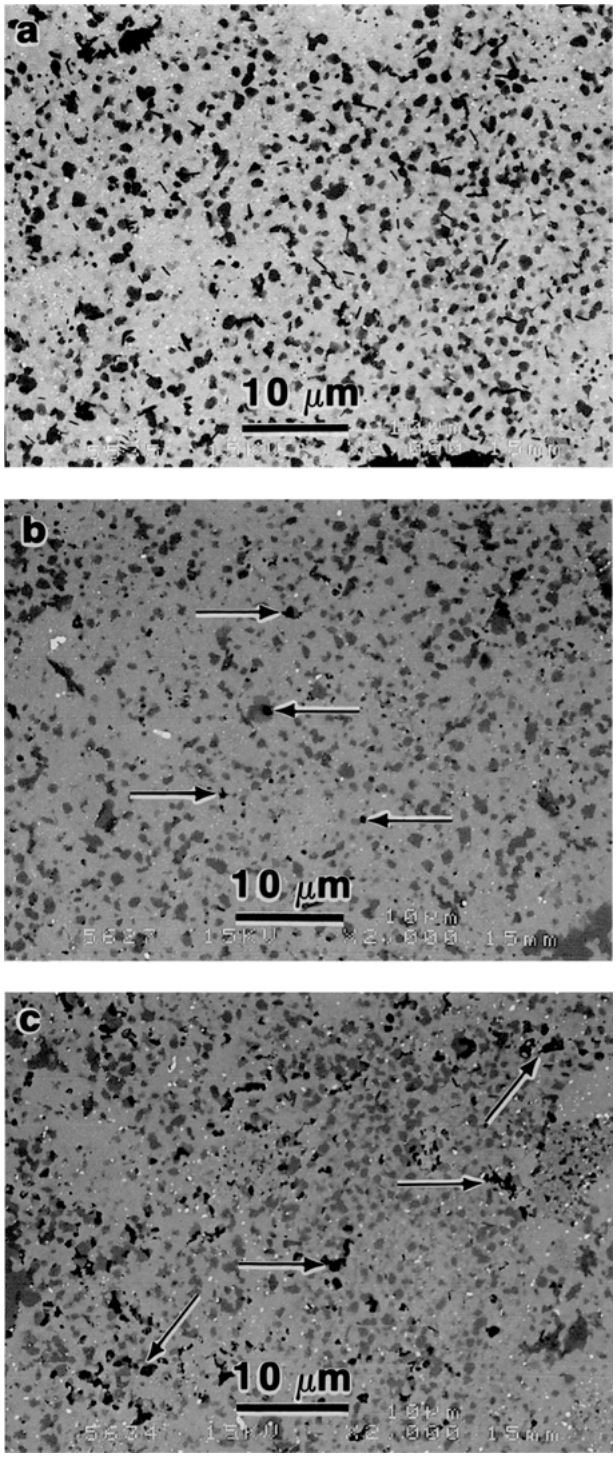

Figure 7 Selected SEM images from the tensile areas (at $\sigma_{el} = 140$ MPa) of the samples tested at (a) 860°C, (b) 900°C and (c) 940°C. Arrows indicate cavities.

smaller ones and in some instances joining up. Ultimately it is this linking up of cavities that leads to failure of the material (creep rupture) as has been shown in other ceramic systems [10–12].

Higher magnification views of the cavities formed in the 940°C material are shown in Fig. 8. The cavities within the fine-grained regions (Fig. 8a) are quite discernible with the larger cavities ranging from about 1 to 2 μm in size. In Fig. 8b an area containing a large dark grey porous TiO_{2-x} agglomerate (typically 20–40 μm in size) shows small cavities dispersed throughout the

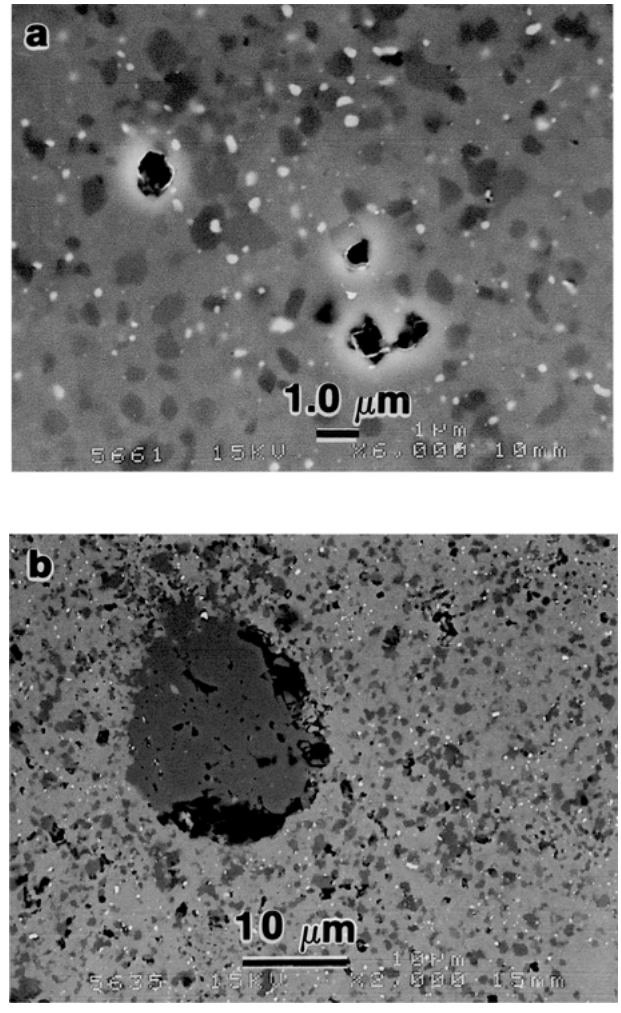

Figure 8 High magnification SEM images from the tensile area of the 940°C sample in Fig. 6 showing cavitation: (a) within the fine-grained region and (b) around a large TiO_{2-x} agglomerate.

fine-grained network, as before, but around the periphery of the TiO_{2-x} inclusion there is noticeable cavity formation and growth (>5 μm in size). At this temperature, an estimate of the critical crack length from fracture toughness measurements [13] is approximately 200 μm, therefore cavities need to grow and link up (allowing for slow crack growth) for catastrophic failure to occur.

4. Discussion

The analysis and microstructural observations of creep damage in the fine-grained synroc material presented in the previous sections suggests that the most plausible mechanism governing creep deformation is primarily grain boundary sliding processes accommodated locally by the opening up of grain boundary cavities on the tensile surfaces as revealed in Figs 7 and 8. The θ-analysis supports the premise that that the deformation mechanism is the same at all stress levels due to the small stress dependence on the activation energy. Further the magnitude of the activation energy is equivalent irrespective of the method of calculation and does not vary significantly with temperature (Table II) indicating that the same creep damage process controls the behaviour.

By contrast despite the observed differences in the stress exponent at 860°C and 900°C ($n = 3.3$) compared to 940°C ($n = 2$), from the Norton power law analysis and supported by the θ-projection analysis (Fig. 6), which point to a possible change in the creep mechanism for this multi-phase fine-grained ceramic, there is no evidence microstructurally to suggest this to be the case. In the review articles compiled by Cannon and Langdon [14, 15] they show that a stress exponent close to 3 is usually interpreted in terms of a glide and climb of dislocations and $n = 2$ generally suggests that grain-boundary sliding is the controlling mechanism based on considerable experimental data of various polycrystalline ceramics and associated theoretical creep models. In the synroc material accommodation by grain boundary sliding intimates that it is considerably enhanced because of the very fine grain structure. The movement of grains is then responsible for the formation of cavities distributed throughout the microstructure at grain boundaries and triple point junctions.

The phase and microstructural characterisation show that there is no indication of liquid phase formation at temperature (Fig. 2), i.e., no diffuse hump in the background of the X-ray spectra, or any discernible change in the microstructure (grain shape or size) apart from the inhomogeneous cavitation that occurs in preferred regions at 900°C and 940°C (Fig. 7b and c). The density and size of these cavities increases with an increase in temperature. Isolated cavities appear to be quite regular in shape whereas other regions, particularly at 940°C (Fig. 8), reveal irregular shaped cavities indicative of a transition to crack-like morphology. These irregular cavities signal the onset of more rapid growth due to the spread in the size, which has clear implications in the creep rupture life of the material. The absence of a liquid phase at these temperatures rules out viscous creep and solution-precipitation mechanisms. Overall the results serve to highlight that cavity-controlled deformation due to grain boundary sliding accounts for most of the creep in this fine-grained complex multiphase synroc ceramic.

In the context of the application of synroc, the upper reaches of planned radioactive waste repository temperatures is significantly lower than those used in this study. As a result the high temperature creep performance of synroc indicates that it is capable of safely withstanding reasonably high temperatures (<860°C) whilst retaining its mechanical integrity even under considerable stresses, and more importantly its behaviour will not lead to radioactive leaching and potential failure. Although the incidence of cavitation could have a profound effect on leach resistance. On a similar note, the stresses the material would likely be subjected to in a repository storage situation would be significantly lower than those used in this work. Nevertheless, the present study has provided useful fundamental data, in particular activation energy values, which provide the basis for constructing models and in design calculations of hot pressing containers that are used in the fabrication of synroc-C. Similarly, the tests have highlighted the temperatures and stresses that determine the creep damage response of this complex, multiphase material. Microstructural studies using TEM are currently being carried out on the creep specimens to verify the creep mechanism and to unequivocally ascertain whether any vitreous phase (thin glassy film) at grain boundaries [2, 7] exists and if so its influence on the creep deformation process. There is scope for more fundamental work in elucidating the effects of microstructural variables in relation to high temperature strength and creep properties in synroc.

5. Conclusion

In this study the high temperature creep behaviour of synroc-C in an Ar atmosphere has been investigated and new information has been gained about the creep damage at the temperatures examined. The creep curves exhibit primary and secondary creep but no tertiary stage and the creep rate increased linearly with applied stress at each temperature over the entire stress range. The creep rates fitted the Norton equation quite well and two creep rate equations were obtained owing to differences in the stress exponents at 860/900°C ($n = 3.3 \pm 0.6$) and 940°C ($n = 2.0 \pm 0.2$). For the temperature range examined, an average activation energy of $Q = (440 \pm 40)$ kJ/mol was obtained. A modified form of the θ-projection equation was used and it was found to adequately describe the creep data and an activation energy of 464 kJ/mol was obtained, in agreement with that from the Norton equation. Accordingly, the activation energy analysis based on θ-values provides a useful extension to the Norton power-law method for describing the influence of stress and temperature on creep. Microstructural examination of creep samples indicate that the creep deformation involved grain boundary sliding to be the active process with extensive cavitation occurring in the material tested at 940°C. The observations suggest that cavitation at grain boundary junctions is not associated with any one phase.

Acknowledgments

The authors wish to express their gratitude to Lou Vance of ANSTO for helpful comments on the manuscript.

References

1. A. E. RINGWOOD, S. E. KESSON, N. G. WARE, W. D. HIBBERSON and A. MAJOR, *Nature* **278** (1979) 219.
2. A. E. RINGWOOD, S. E. KESSON, K. D. REEVE, D. M. LEVINS and E. J. RAMM, in "Radioactive Waste Forms for the Future," edited by W. Lutze and R. C. Ewing (Elsevier, Amsterdam, 1988) p. 233.
3. E. G. MEHRTENS and K. U. SNOWDEN, *J. Mater. Sci.* **35** (2000) 4207.
4. B. A. LATELLA and T. LIU, *J. Amer. Ceram. Soc.* **84** (2001) 117.
5. G. W. HOLLENBERG, G. R. TERWILLIGER and R. S. GORDON, *ibid.* **54** (1971) 196.
6. B. F. DYSON and T. B. GIBBONS, *Mater. Sci. Tech.* **9** (1993) 151.
7. G. R. LUMPKIN, K. L. SMITH and M. G. BLACKFORD, *J. Mater. Res.* **6** (1991) 2218.
8. R. W. EVANS, T. MURAKAMI and B. WILSHIRE, *Brit. Ceram. Trans. J.* **87** (1988) 54.

9. R. W. EVANS and B. WILSHIRE, "Introduction to Creep" (The Institute of Materials, London, 1993).
10. P. LIPETZKY, S. R. NUTT, D. A. KOESTER and R. F. DAVIS, *J. Amer. Ceram. Soc.* **74** (1991) 1240.
11. D. S. WILKINSON, *ibid.* **81** (1998) 257.
12. R. F. KRAUSE, W. E. LUECKE, J. D. FRENCH, B. J. HOCKEY and S. M. WIEDERHORN, *ibid.* **82** (1999) 1233.
13. E. G. MEHRTENS and K. U. SNOWDEN, unpublished work, 1994.
14. W. R. CANNON and T. G. LANGDON, *J. Mater. Sci.* **18** (1983) 1.
15. *Idem.*, *ibid.* **23** (1988) 1.

Received 22 October 2002
and accepted 20 May 2003